

This is an Open Access document downloaded from ORCA, Cardiff University's institutional repository:<https://orca.cardiff.ac.uk/id/eprint/143806/>

This is the author's version of a work that was submitted to / accepted for publication.

Citation for final published version:

Chen, Huanhao, Chansai, Sarayute, Xu, Shaojun, Xu, Shanshan, Mu, Yibing, Hardacre, Christopher and Fan, Xiaolei 2021. Dry reforming of methane on bimetallic Pt–Ni@CeO₂ catalyst: a in situ DRIFTS-MS mechanistic study. *Catalysis Science & Technology* 11 (15) , pp. 5260-5272. 10.1039/D1CY00382H

Publishers page: <http://dx.doi.org/10.1039/D1CY00382H>

Please note:

Changes made as a result of publishing processes such as copy-editing, formatting and page numbers may not be reflected in this version. For the definitive version of this publication, please refer to the published source. You are advised to consult the publisher's version if you wish to cite this paper.

This version is being made available in accordance with publisher policies. See <http://orca.cf.ac.uk/policies.html> for usage policies. Copyright and moral rights for publications made available in ORCA are retained by the copyright holders.



Dry reforming of methane on bimetallic Pt–Ni@CeO₂ catalyst: a in situ DRIFTS-MS mechanistic study†

Huanhao Chen,^a Sarayute Chansai,^b Shaojun Xu,^{b,cd} Shanshan Xu,^b Yibing Mu,^b Christopher Hardacre^b and Xiaolei Fan^b

Bimetallic Pt–Ni catalysts can promote catalytic dry reforming of methane (DRM) with improved activity and deactivation resistance compared to the relevant monometallic catalysts. Further development of Pt–Ni catalysts requires mechanistic insights into the catalytic system. Herein, a mechanistic study of DRM over Pt–Ni supported on cerium oxide catalysts (i.e., Pt–Ni@CeO₂) was performed using in situ coupled diffuse reflectance infrared Fourier-transform spectroscopy and mass spectrometry (DRIFTS-MS). Specifically, a comparative study of DRM over Pt–Ni@CeO₂ and control materials under continuous temperature ramping, isothermal steady-state and fast cycling transient conditions was conducted to gain information on the key surface active intermediates. As compared with the Ni@CeO₂ monometallic catalyst, the bimetallic Pt–Ni@CeO₂ catalyst showed significantly enhanced performance regarding activity, H₂/CO ratio and long-term stability. In situ DRIFTS measurements revealed that CH₄ decomposition on the surface of monometallic Ni phases readily caused serious coke deposition and deactivation. Conversely, the Pt phase in the bimetallic catalyst could improve CO₂ dissociation, thus producing adsorbed oxygen species, which are beneficial for oxidising surface carbon species (derived from CH₄ decomposition) to reduce coke formation. Meanwhile, the existence of Pt sites in the bimetallic catalyst could significantly improve metal dispersion, and thus facilitate the decomposition of CH₄.

1. Introduction

Catalytic dry reforming of methane (i.e., DRM, CH₄ + CO₂ → 2CO + 2H₂, Δ_rH⁰_{298K} = 247 kJ mol⁻¹) converts two major greenhouse gases (i.e., CO₂ and CH₄) to produce syngas (i.e., CO and H₂).^{1–4} DRM processes over supported metal catalysts require relatively high temperatures (e.g., >600 °C), in order to achieve the desirable conversions, due to its endothermic nature, which commonly results in metal sintering and/or carbon deposition, and hence catalyst deactivation.^{5–7} Accordingly, to overcome the limitation, the design and

development of (i) thermally stable catalysts with good anti-sintering and -coking properties for conventional high-temperature operations and/or (ii) highly active catalysts at low temperatures are necessary to promote DRM further toward practical applications.

Supported nickel (Ni) catalysts are common reforming catalysts used for DRM due to their good activity, high availability and low cost, having the potential for large-scale industrial applications.^{8–11} However, it is well-known that the major limitations of Ni-based reforming catalysts are metal sintering and coke deposition during catalysis, especially under severe conditions.¹² Many strategies have been proposed and developed to address these limitations, for example, the addition of a secondary noble metal phase, such as Pt,^{13–17} Rh,^{18,19} or Ru,^{20,21} in Ni catalysts to improve the resistance to metal sintering and coking. For example, Araiza et al.²² recently studied the effect of the metal composition (i.e., Pt/Ni atomic ratio) in the bimetallic Pt–Ni/CeO₂ catalyst on the activity and stability, revealing that Pt doping significantly improved the anti-sintering and anti-coking properties of the Ni catalyst. Specifically, the improvement of catalytic properties was attributed to the promoting effect of Pt doping on Ni, which improved the Ni dispersion. It is worth mentioning that cerium oxide (CeO₂), as the catalyst

^a State Key Laboratory of Materials-Oriented Chemical Engineering, College of Chemical Engineering, Nanjing Tech University, Nanjing 210009, China. E-mail: h.chen@njtech.edu.cn

^b Department of Chemical Engineering and Analytical Science, School of Engineering, The University of Manchester, M13 9PL, UK.

E-mail: c.hardacre@manchester.ac.uk, xiaolei.fan@manchester.ac.uk

^c School of Chemistry, Cardiff University, Main Building, Park Place, Cardiff, CF10 3AT, UK

^d UK Catalysis Hub, Research Complex at Harwell, Rutherford Appleton Laboratory, Harwell, Oxon OX11 0FA, UK

support, also has the ability to prevent coke deposition and improve the stability of reforming catalysts due to its abundant lattice oxygen and remarkable redox properties. Accordingly, fundamental understanding of DRM catalysis over these catalysts is necessary for the purpose of further optimisation and development of DRM catalysts.

In situ diffuse reflectance infrared Fourier-transform spectroscopy (DRIFTS) techniques have been shown to be powerful tools in the study of the mechanisms of surface reactions during catalysis such as DRM,^{7,12,23,24} hydrocarbon selective catalytic reduction (HC-SCR) of NO_x,^{25–28} CO₂ hydrogenation^{29,30} and the Fischer–Tropsch process.³¹ Specifically, by coupling mass spectrometry, that is, DRIFTS-MS, the in situ technique can provide information on not only the chemical nature and surface dynamics of reactive species on a catalyst (microscopic) but also the simultaneous evolution of reactant/product compositions as a function of time-on-stream (ToS, macroscopic).^{26–28} Conventional in situ DRIFTS-MS characterisation is performed under steady-state conditions,²⁸ making it difficult to capture and identify the key intermediates due to (i) the transient nature of some surface species and (ii) accumulation of the species with similar chemical properties on the surface of metal catalysts and/or catalyst supports. Therefore, catalytically important changes and the associated mechanistic information on surface species could be overlooked.²⁸ Conversely, the fast cycling transient in situ DRIFTS-MS technique, which was operated under short time-on-stream (STOS) conditions,^{26,28,32–34} showed the capability of detecting and identifying the evolution of surface active species adsorbed in the timeframe of seconds rather than minutes.³² For example, the transient technique was applied to investigate the mechanisms of the H₂-assisted HC-SCR reaction over the

Ag/Al₂O₃ catalyst, revealing that only the isocyanate species adsorbed on the aluminium sites close to Ag were the possible intermediates in the H₂-assisted HC-SCR. In contrast, this information was not able to be obtained under steady-state conditions due to the adsorption of chemically equivalent species on both the surface of the metal and support hiding the dynamics of possibly real key intermediates.²⁸

Herein, this work presents a comprehensive in situ DRIFTS-MS study of catalytic DRM over the bimetallic Pt–Ni supported on CeO₂ catalyst (i.e., Pt–Ni@CeO₂) under temperature-ramping, isothermal steady-state and fast cycling transient conditions. This comparative work aims to identify the nature and role of surface-active intermediates in DRM, and hence gain insights into the mechanism and reaction pathway of DRM, being beneficial to advance the catalysis.

2. Experimental

Catalyst preparation

A bimetallic Pt–Ni@CeO₂ catalyst with a Pt/Ni atomic ratio of 1 : 3 was prepared by an incipient wetness impregnation method according to the literature.²² The Pt/Ni ratio (corresponding to w/w of 1 : 1) was previously proved as the optimum ratio for enabling the comparatively best catalytic performance in DRM.²² Specifically, cerium oxide (CeO₂, Sigma-Aldrich, ≥99.0%) was co-impregnated with nickel (II) chloride (NiCl₂, Sigma-Aldrich, 98%) and chloroplatinic acid hexahydrate (H₂-PtCl₆, Sigma-Aldrich, ≥37.50% Pt basis) aqueous solution for 12 h and dried at 80 °C. Then the obtained catalyst was calcined in a muffle furnace at 500 °C in flowing air for 2 h with a heating rate of 5 °C min⁻¹. A reference CeO₂ supported Ni catalyst (i.e., Ni@CeO₂) was also prepared using NiCl₂ as a metal precursor via the same experimental procedures. The total metal loading of the catalysts under study was set to 2 wt%, while the actual metal loadings are listed in Table S1 in the ESI,† which was determined by inductively coupled plasma optical emission spectroscopy (ICP-OES). TEM analysis of the as-prepared catalysts shows that the sizes of the metallic phases in the three catalysts are comparable (Fig. S1†).

Catalytic DRM

Catalytic DRM over the catalysts was evaluated in a continuous-flow fixed-bed stainless-steel reactor (6 mm O.D. × 4 mm I.D.) under atmospheric pressure, and the experimental rig is shown in Fig. 1. Specifically, for each experiment, ~200 mg of the as-prepared Ni@CeO₂ or Pt–Ni@CeO₂ catalyst (pelletised with particle sizes of 250–425 μm) was packed in the middle of the reactor sandwiched by two quartz wool beds, where a K-type thermocouple was embedded in the catalyst bed to measure the actual temperature of the catalyst bed during the catalysis. Prior to reaction, the catalyst was reduced in situ with a flow of 20 vol% H₂/Ar (50 mL min⁻¹) at 600 °C for 1 h. H₂-TPR analysis of the catalysts showed that all the catalysts could be fully reduced at <600 °C (Fig. S2†). Thereafter, the catalyst was heated up to 650 °C (at 10 °C min⁻¹) under argon (Ar, at 50 mL min⁻¹) and purged for 15 min, followed by feeding the reaction gas mixture



Huanhao Chen

Dr Huanhao Chen is a Professor in the State Key Laboratory of Materials-Oriented Chemical Engineering and College of Chemical Engineering at Nanjing Tech University, China. He received his Ph.D. in Chemical Engineering from South China University of Technology in 2014. After that, he continued his research as a Postdoctoral Scholar Research Associate in the area of heterogeneous catalysis and reaction engineering at

University of Puerto Rico and University of Southern California, United States. From 2018 to 2020, he served as a Marie Curie Fellow at the University of Manchester, United Kingdom, worked on the non-thermal plasma catalysis and catalytic reaction engineering. He has been awarded the Marie Curie Individual Fellowship by the European Commission.

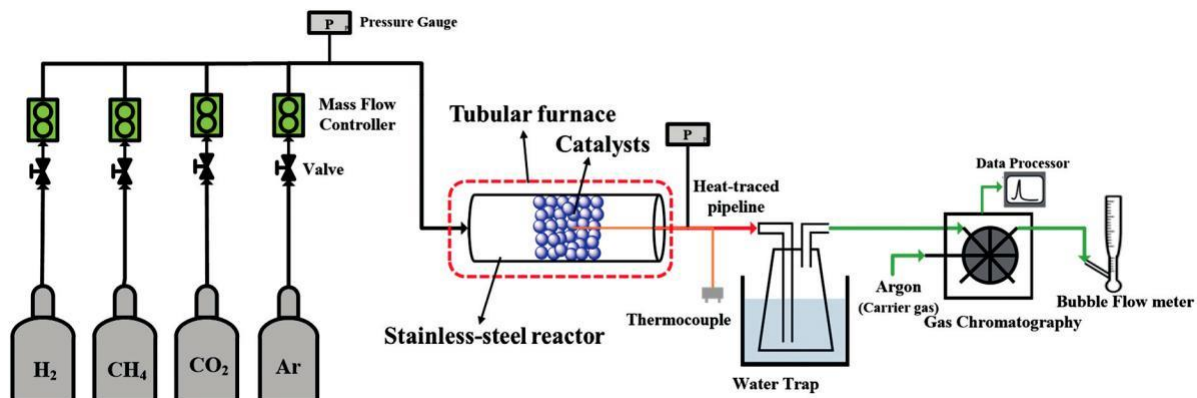


Fig. 1 Schematic diagram of the experimental rig for catalytic DRM.

(45 vol% CO₂/45 vol% CH₄/10 vol% Ar) with a total flow rate of 60 ml min⁻¹ into the reactor, which was controlled by three mass flow controllers (Bronkhorst®, F-201CV-500-RAD-11-V). Longevity test was performed at 650 °C over 45 h time-on-stream (ToS). The blank experiment over the bare CeO₂ support was also conducted under the same conditions for reference. The effluent gas from the reactor was analysed using a gas chromatograph (GC, PerkinElmer, Clarus® 590) equipped with an Elite-Carbon molecular sieve packed column (N9303926), a methaniser, a thermal conductivity detector (TCD) and a flame ionisation detector (FID). Samples were collected via an automated six-way valve containing a sample loop until at least three consecutive measurements were in a margin of error of ~3%. Liquid products (e.g., water) generated from the reaction were removed cumulatively from the outlet stream using a water trap cooled by an ice bath. The gas flow rate in the outlet of the reactor was measured using a bubble-flow meter in order to determine the CO₂ conversion (X_{CO_2} , eqn (1)), CH₄ conversion (X_{CH_4} , eqn (2)), and H₂/CO molar ratio (R_{SG} , eqn (3)).

$$X_{CO_2} \% \frac{1}{4} \frac{F_{CO_2}^{in} - F_{CO_2}^{out}}{F_{CO_2}^{in}} \times 100 \quad (1)$$

$$X_{CH_4} \% \frac{1}{4} \frac{F_{CH_4}^{in} - F_{CH_4}^{out}}{F_{CH_4}^{in}} \times 100 \quad (2)$$

$$R_{SG} \frac{1}{4} \frac{F_{H_2}}{F_{CO}^{out}} \quad (3)$$

where F represents the molar flow rate in the inlet (superscript in) and outlet (superscript out) of the reactor (mol s⁻¹), and the subscript gives the relevant gaseous reactants/products detected by GC.

In situ DRIFTS-MS characterisation

In situ DRIFTS-MS characterisation of the surface chemistry during DRM was performed using a Bruker Tensor 27 FTIR spectrometer coupled with a Hidden Analytical HPR20 mass

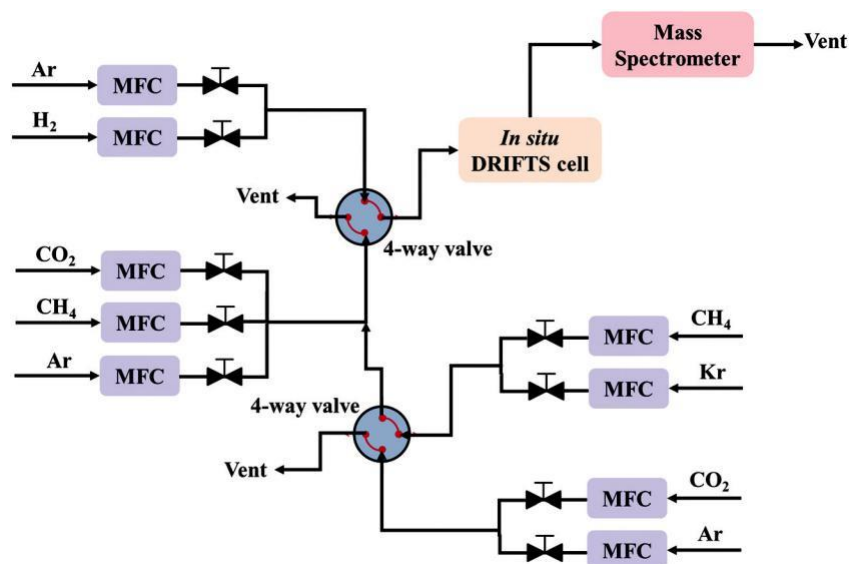


Fig. 2 Schematic diagram of the DRIFTS-MS system for investigating catalytic DRM.

spectrometer (details of the DRIFTS protocols with the gas feed arrangements are shown in Fig. 2), which has been detailed elsewhere.^{28,32} Specifically, the gas flow mixtures were controlled by independent mass flow controllers (Brooks) and introduced into the in situ DRIFTS cell via two 4-way valves which allowed a sharp switch between the two gas mixtures in less than 200 ms.³² Before the DRIFTS analysis, the catalysts (fine powders on the top and pellets with sizes of 250–425 μm on the bottom) were loaded into a ceramic crucible in the cell, and pre-treated at 600 $^{\circ}\text{C}$ for 1 h in a 10% H_2/Ar flow. Under temperature-ramping conditions, the background spectra were collected at 50 $^{\circ}\text{C}$ under Ar prior to the introduction of gas reactants. Subsequently, a gas mixture with a total flow rate of 50 mL min^{-1} (10 vol% $\text{CO}_2/10$ vol% $\text{CH}_4/80$ vol% Ar) was introduced into the cell, and the evolution of the DRIFT spectra during catalysis was recorded at every ~ 56 s with a resolution of 4 cm^{-1} by ramping the temperature of the catalyst bed from 50 to 600 $^{\circ}\text{C}$ at 10 $^{\circ}\text{C min}^{-1}$. After that, the gas mixture (10 vol% $\text{CO}_2/10$ vol% $\text{CH}_4/80$ vol% Ar) was introduced into the cell under isothermal conditions at 550 $^{\circ}\text{C}$, and the DRIFT spectra were recorded every ~ 56 s with a resolution of 4 cm^{-1} for 20 min. Two different sets of fast cycling transient experiments were performed. The first set of experiments was designed to switch the gas mixtures at a constant flow rate of 50 mL min^{-1} between 10 vol% $\text{CO}_2/90$ vol% Ar and 10 vol% $\text{CH}_4/30$ vol% Kr/60 vol% Ar (where krypton, Kr, was used as the reference). The second set of experiments allowed the switch of the gas mixtures at a constant flow rate of 50 mL min^{-1} between 10 vol% $\text{CO}_2/90$ vol% Ar and 10 vol% $\text{CO}_2/10$ vol% $\text{CH}_4/30$ vol% Kr/50 vol% Ar. For both experiments, the switch (of feeds) was performed for 20 cycles with a short duration of 1 min for each cycle. Specifically, for each cycle, DRIFT spectra were recorded every 10 s with a resolution of 4 cm^{-1} and analysed using OPUS software provided by Bruker. The background spectra were collected at 550 $^{\circ}\text{C}$ under Ar without any gases to correct the spectra obtained from

DRIFTS experiments under steady state and transient conditions. During the experiments, the exit of the DRIFTS cell was connected to a MS in order to record the evolution of the gas phase species, i.e. CO_2 ($m/z = 44$), H_2 ($m/z = 2$), CH_4 ($m/z = 15$), CO ($m/z = 28$), H_2O ($m/z = 18$) and Kr ($m/z = 82$), with a response time less than 1 s.

3. Results and discussion

Catalytic DRM performances

To assess the catalytic performance of the catalysts, longevity tests of the Ni@CeO_2 and Pt-Ni@CeO_2 catalysts for DRM were performed at 650 $^{\circ}\text{C}$ as a function of ToS, and the results are presented in Fig. 3. The monometallic Ni@CeO_2 catalyst presented low initial CO_2/CH_4 conversions of about 24% and 11%, respectively, as shown in Fig. 3a. Thereafter, the monometallic Ni@CeO_2 catalyst deactivated rapidly, over 10 h on stream and the CO_2/CH_4 conversions of the catalyst dropped by $\sim 60\%$ and $\sim 75\%$, respectively. In addition, over 8 h ToS, the molar ratio of H_2/CO decreased rapidly from ~ 0.2 to almost zero. Comparatively, the monometallic Pt@CeO_2 demonstrated a stable performance in DRM (Fig. 3b) with the CO_2 conversion decreasing by about 8% during the test. Although relatively stable catalytic performance was achieved by Pt@CeO_2 , the reaction was terminated due to physical blocking of the packed bed (with the measured pressure drop >2 bar), which was caused by carbon deposition in between catalyst pellets rather than on the metal surface.³⁵ Conversely, as shown in Fig. 3c, the bimetallic Pt-Ni@CeO_2 catalysts showed significantly stable performance in DRM without deactivation compared to the monometallic catalysts, especially Ni@CeO_2 . It is worth mentioning that, although the monometallic Pt catalyst (Pt@CeO_2) was also very active, it is less attractive compared to the bimetallic Pt-Ni@CeO_2 from an economic perspective. Fig. S3† shows that, over the ToS of 45 h, the Pt-Ni@CeO_2 catalyst presented a rather stable performance with CO_2/CH_4

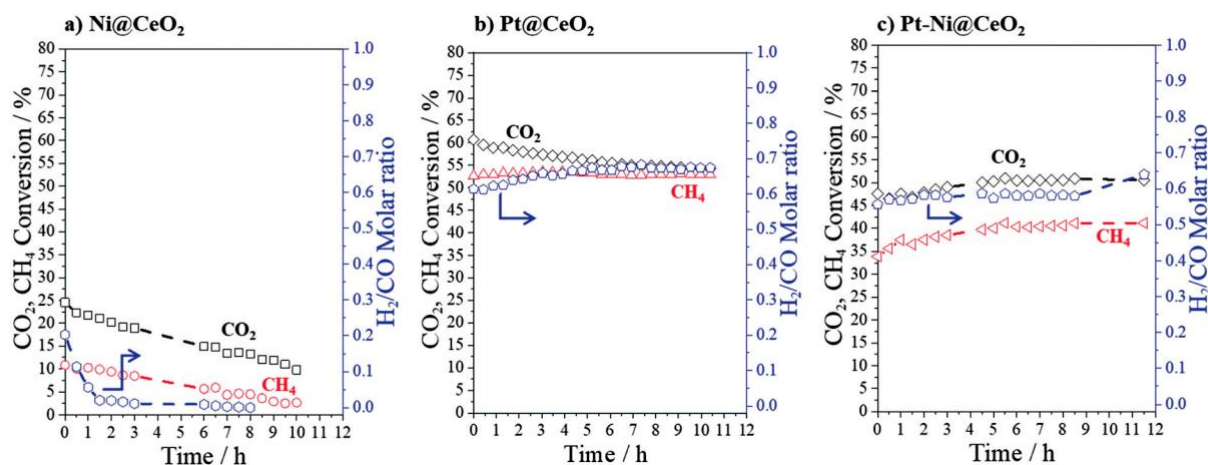


Fig. 3 Catalytic DRM performances of the catalysts regarding the CO_2/CH_4 conversions and H_2/CO molar ratio as a function of ToS: (a) Ni@CeO_2 , (b) Pt@CeO_2 , and (c) Pt-Ni@CeO_2 . (Experimental conditions: feed gas = 45 vol% $\text{CO}_2/45$ vol% $\text{CH}_4/10$ vol% Ar, total flow rate = 60 mL (STP) min^{-1} , temperature = 650 $^{\circ}\text{C}$).

(characterised by the IR bands in the region of 1310–1670 cm^{-1} , shaded by the red rectangle).^{7,37} Specifically, as shown in Fig. 4c(left), for the Pt–Ni@CeO₂ catalyst, the intensity of the IR band at $\sim 2050 \text{ cm}^{-1}$ (that is, the linearly coordinated CO species on metallic Pt sites, shaded by the purple rectangle) decreased progressively as a function of temperature ($>400 \text{ }^\circ\text{C}$), indicating that the linear carbonyls could be the key surface active intermediate. For the Pt@CeO₂ catalyst, the intensity of linearly coordinated CO species on Pt sites ($\sim 2050 \text{ cm}^{-1}$) also decreased progressively as a function of temperature ($>400 \text{ }^\circ\text{C}$), while the intensity of the IR band at $\sim 1860 \text{ cm}^{-1}$ (that is, the bridged CO species on Pt sites, shaded by the grey rectangle) remained relatively stable. The corresponding MS profiles (Fig. 4b and c, right) showed that Pt@CeO₂ and Pt–Ni@CeO₂ were more active than Ni@CeO₂ in DRM (Fig. 4a, right). Specifically, over the Pt–Ni@CeO₂ catalyst, signals at $m/z = 28$ (corresponding to CO) and $m/z = 2$ (corresponding to H₂), were observed at about 20 and 25

min, respectively, much quicker than found for the Ni@CeO₂ catalyst (i.e., ca. 40 and 42.5 min, respectively). The catalytic performances measured by DRIFTS-MS are highly consistent with the results measured in the plug-flow reactor of this work (Fig. 3), as well as previous findings.²²

Steady-state in situ DRIFTS-MS studies. Under isothermal conditions at 550 $^\circ\text{C}$ (dwell time = 20 min for each experiment), DRIFT-MS characterisation of the catalysis was performed as a function of ToS. It was found that DRM could be started over the catalysts under investigation at 450 $^\circ\text{C}$ (Fig. S4†), and hence 550 $^\circ\text{C}$ was appropriate for studying the surface reactions of DRM since an increase in the reaction temperature might only accelerate the rate rather than varying the reaction pathways when the catalysts were active. As shown in Fig. S6a,† for the bare CeO₂ support, in situ DRIFT spectra revealed that, upon the switching from pure Ar to CO₂/CH₄ mixture, the IR band intensity of carbonate-like species (shaded by the red rectangle) increased over the first 5 min, and then stabilised. Specifically, the variation of

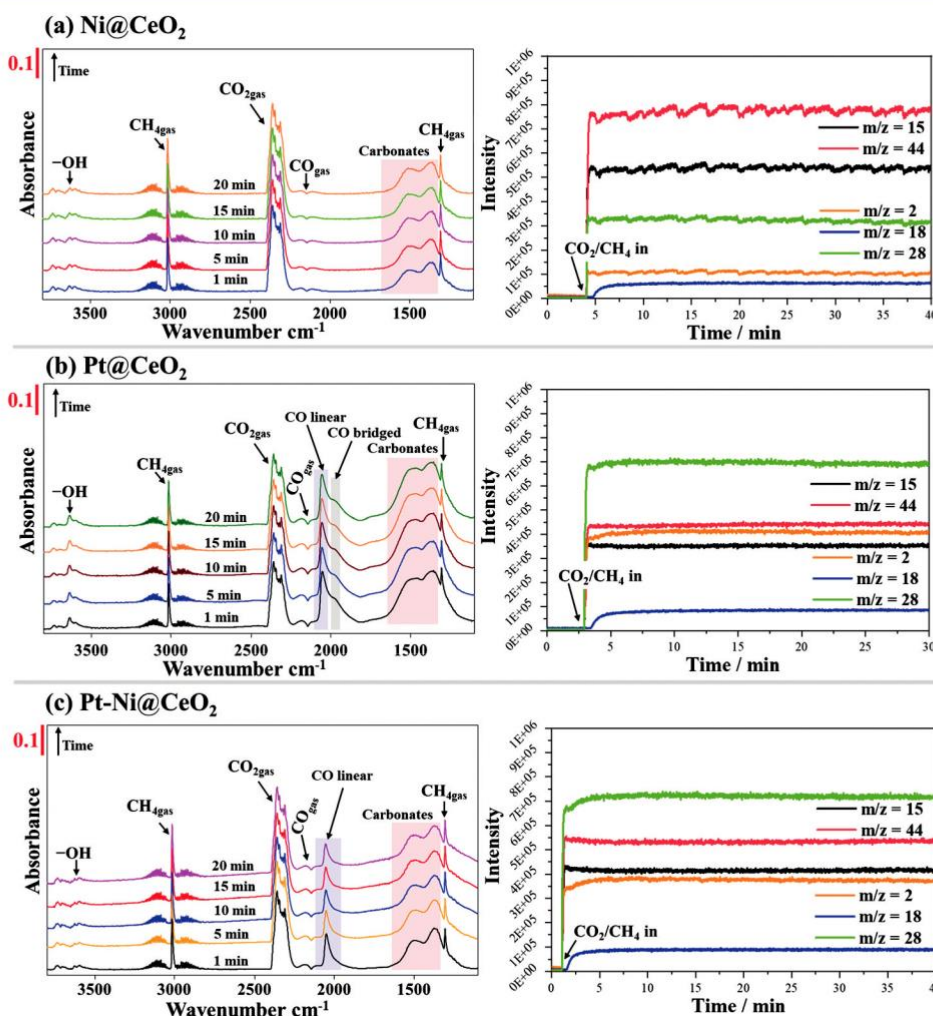


Fig. 5 In situ DRIFTS spectra of the catalysis over the catalysts and corresponding MS signals collected at the exit of the DRIFTS cell as a function of ToS during DRM at 550 $^\circ\text{C}$: (a) Ni@CeO₂, (b) Pt@CeO₂, and (c) Pt–Ni@CeO₂. (Experimental conditions: feed gas = 10 vol%CO₂/10 vol%CH₄/80 vol% Ar, total flow rate = 50 mL (STP) min^{-1}).

IR signals of -OH groups ($\sim 3635\text{ cm}^{-1}$), the gaseous CO_2 ($\sim 2349\text{ cm}^{-1}$) and CH_4 (~ 3016 and 1305 cm^{-1}) remained constant as a function of ToS. Correspondingly, MS profiles confirmed that CeO_2 could only produce trace amounts of CO and H_2 in the system (Fig. S6b†), which is consistent with the findings from the temperature-ramping experiment (Fig. S5†).

For the Ni@CeO_2 catalyst with the reactant mixture, as observed in Fig. 5a(left), variation of the intensity of IR bands of gaseous CO ($2110\text{--}2235\text{ cm}^{-1}$), -OH groups ($\sim 3635\text{ cm}^{-1}$) and surface carbonate-like species (shaded by red rectangle) was insignificant under isothermal conditions at $550\text{ }^\circ\text{C}$. Conversely, with the introduction of the CO_2/CH_4 mixture to the system (Fig. 5b and c, left), the evolution of surface species was recorded for the Pt@CeO_2 and Pt-Ni@CeO_2 catalysts, i.e. the intensity of IR bands at the region between ~ 1443 and 1670 cm^{-1} (i.e., bidentate carbonates,^{7,23,37,38} shaded by the red rectangle) and the linear carbonyls decreased slightly, respectively, suggesting the possible key role of these surface species played in DRM. However, it is worth noting that the IR band intensity of gas phase CO ($2110\text{--}2235\text{ cm}^{-1}$) and polydentate carbonate species ($1310\text{--}1443\text{ cm}^{-1}$,^{7,38} shaded by the red rectangle) remained stable, suggesting that polydentate carbonates could be the spectators (which will be discussed later). It is worth noting that the intensity of carbonates adsorbed on the surface of all catalysts was significantly weaker than that of the bare CeO_2 (Fig. S6a†), confirming that the carbonate species adsorbed predominantly on the support rather than the metal sites of the catalysts, agreeing with previous findings.²³

The corresponding MS profiles (Fig. 5b and c, right) further confirmed the comparatively better performance of the Pt@CeO_2 and Pt-Ni@CeO_2 catalysts than that of the Ni@CeO_2 catalyst (Fig. 5a, right), e.g. the relevant MS signal intensities of CO ($\sim 7 \times 10^5$) and H_2 ($\sim 3.5 \times 10^5$) for Pt-Ni@CeO_2 were much higher than those for Ni@CeO_2 (i.e., $\sim 3.2 \times 10^5$ for CO and $\sim 1 \times 10^5$ for H_2) under steady-state conditions. For all catalysts, the MS signals showed the rapid production of CO and H_2 before reaching the steady-state at $550\text{ }^\circ\text{C}$, reflecting the immediate start of DRM over them and the associated population of surface species within the time scale of ~ 1 min. Consequently, in situ transient experiments are needed in order to gain further information on the reaction mechanism, which will be discussed later. Lastly, H_2O ($m/z = 18$) was also produced by the systems over all catalysts, suggesting the possible occurrence of the reversed water gas shift (RWGS) reaction⁷ in the current system.

Fast cycling transient in situ DRIFTS-MS studies. To identify the active surface intermediates, catalytic DRM over the Ni@CeO_2 and Pt-Ni@CeO_2 catalysts under investigation and the bare CeO_2 support was evaluated by fast cycling transient in situ DRIFTS-MS at $550\text{ }^\circ\text{C}$, in which the surface dynamics and bulk gas composition of the catalytic system were examined with the periodically fast switching of the feed stream between $10\%\text{CO}_2/\text{Ar}$ and $10\%\text{CO}_2/10\%\text{CH}_4/30\%\text{Kr}/\text{Ar}$ (dwell time = 1 min for each cycle, 20 cycles). The Pt@CeO_2 catalyst was not further investigated since it is less attractive as compared with Pt promoted Ni catalysts (here, i.e., Pt-Ni@CeO_2), considering the cost implications. As shown in Fig. S7,† under the transient conditions of switching the gas

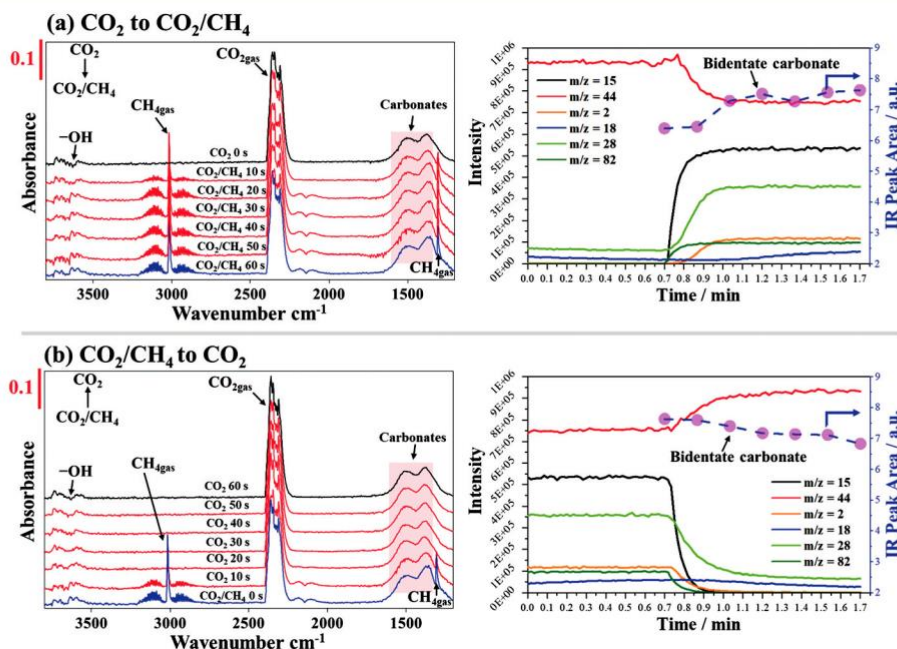


Fig. 6 In situ DRIFT spectra over the Ni@CeO_2 catalyst and corresponding MS signals collected at the exit of the DRIFTS cell and the evolution of surface bidentate carbonate and linear carbonyls as a function of ToS during the 1st cycle of DRM switching between CO_2 and CO_2/CH_4 feeds at $550\text{ }^\circ\text{C}$: (a) CO_2 to CO_2/CH_4 , and (b) CO_2/CH_4 to CO_2 . (Experimental conditions: feed gases = $10\text{ vol}\%\text{CO}_2/90\text{ vol}\%\text{Ar}$ and $10\text{ vol}\%\text{CO}_2/10\text{ vol}\%\text{CH}_4/30\text{ vol}\%\text{Kr}/50\text{ vol}\%\text{Ar}$, total flow rate = $50\text{ mL (STP) min}^{-1}$).

feeds, in situ DRIFT spectra collected during the 1st and 2nd cycle showed that the IR band intensity of surface carbonates on bare CeO₂ (1310–1670 cm⁻¹, shaded by the red rectangle) remained constant. Correspondingly, upon switching to the CO₂/CH₄ mixture in the system, the MS profiles, again, showed the production of trace amounts of CO and H₂ during each cycle (Fig. S8†).

As shown in Fig. 6a, under the CO₂/Ar stream (during the 1st cycle), IR band peaks in the region of 1310–1670 cm⁻¹ (shaded by the red rectangle) were observed, confirming the formation of carbonate-like species on the surface of the Ni@CeO₂ and Pt–Ni@CeO₂ catalysts. The formation of linear carbonyls on the surface of Pt–Ni@CeO₂ was identified as well, which might be mainly attributed to the CO₂ dissociation on Pt.³⁹ On switching from CO₂ to the CO₂/CH₄ mixture (the switching point was referenced by the occurrence of a Kr signal, *m/z* = 82), for both catalysts, the integrated peak area of bidentate carbonates (Fig. 6a and 7a, right) did not show significant changes. However, for the Pt–Ni@CeO₂ catalyst, the IR band intensity and peak area of linear carbonyls increased during the first 20 s and then became constant, suggesting the possible contribution of CO₂ and CH₄ to the formation of these species. The increase in the band intensity related to the –OH groups upon the feed of CO₂/CH₄ could be attributed to the reaction between atomic H (dissociated from CH₄) and O (donated by the CeO₂ support²³). For the Pt–Ni@CeO₂ catalyst (Fig. 7a), the MS profiles showed the instantaneous and simultaneous increase in the CO and H₂ MS signals upon the feed of the CO₂/CH₄ mixture. Conversely, the rate of evolution of CO and H₂ MS

signals from the system with the Ni@CeO₂ catalyst was reduced. Regarding the systems under study (over Ni@CeO₂, Pt–Ni@CeO₂ and CeO₂) with CO₂, the associated MS profiles confirmed the formation of CO from the systems (with an intensity of ~0.75 × 10⁵), which could be attributed to the decomposition of weakly adsorbed carbonates on the surface of CeO₂.²³ Additionally, upon switching CO₂ to CO₂/CH₄, a trace amount of H₂O was detected in the systems with the Ni@CeO₂ and Pt–Ni@CeO₂ catalysts, suggesting the occurrence of RWGS.

On switching the CO₂/CH₄ mixture back to CO₂ (during the 1st cycle), as observed in Fig. 6b and 7b, the DRIFTS-MS results showed a nearly reversible phenomenon for the systems over both Ni@CeO₂ and Pt–Ni@CeO₂ catalysts. In addition, Fig. S9–S12† present the variation of IR spectra over the two catalysts and corresponding MS signals collected during the selected 2nd, 10th, and 20th cycles of experiments with the periodically switched feed gas mixtures between CO₂ and CO₂/CH₄, showing the repeatable results.

To further confirm the active surface intermediates, transient experiments were also performed by switching the feeds between 10%CO₂/Ar and 10%CH₄/30% Kr/Ar (dwell time = 1 min for each cycle, 20 cycles). Over the CeO₂ support (Fig. S13a†), upon switching the gas feed from CO₂ to CH₄, the intensity of surface bidentate carbonates (at ~1570 cm⁻¹) decreased rapidly within 20 s, which was also matched by the change in the peak of gaseous CO₂ (at ~2349 cm⁻¹). The corresponding MS profiles showed a decrease in the CO signal upon switching CO₂ to CH₄ (Fig. S14†), indicating that the formation of CO was due to the dissociation of surface

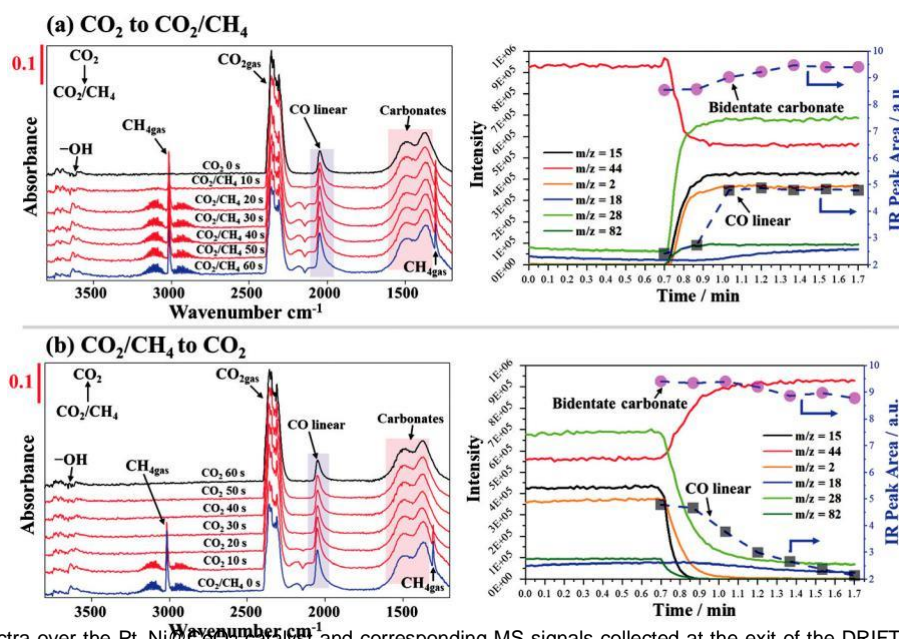


Fig. 7 In situ DRIFT spectra over the Pt–Ni@CeO₂ catalyst and corresponding MS signals collected at the exit of the DRIFTS cell and the evolution of surface bidentate carbonate and linear carbonyls as a function of ToS during the 1st cycle of DRM switching between CO₂ and CO₂/CH₄ feeds at 550 °C: (a) CO₂ to CO₂/CH₄, and (b) CO₂/CH₄ to CO₂. (Experimental conditions: feed gas = 10 vol%CO₂/90 vol% Ar and feed gas = 10 vol%CO₂/ 10 vol%CH₄/30 vol% Kr/50 vol% Ar, total flow rate = 50 mL (STP) min⁻¹).

carbonates formed by CO₂ binding with lattice oxygen of CeO₂. Additionally, in the absence of CO₂, H₂ was not detected by MS. Together with the previous findings and discussion (i.e., Fig. S8†), they confirm the ability of CeO₂ for catalytic DRM. Accordingly, for the specific system, the route of CO formation could be two-fold via the gas-phase DRM and the interaction between CO₂ and the CeO₂ support.

For the Ni@CeO₂ and Pt–Ni@CeO₂ catalyst (Fig. 8a and 9a), upon the introduction of CH₄ after CO₂ saturation (during the 1st cycle), similar surface dynamics were recorded. Specifically, (i) the IR band intensity and integrated peak area of the surface bidentate carbonate (1443–1670 cm⁻¹) decreased as a function of time, which confirms that they were active intermediates to be quickly transformed or consumed by reacting with CH₄; (ii) the IR bands of polydentate carbonate species (1310–1443 cm⁻¹) remained stable, which indicates that they were possible spectators, as reported previously;⁷ and (iii) the increase in the number of

–OH groups was possibly due to the reaction between the atomic hydrogen and oxygen donated by CeO₂, which verifies the hypothesis above. In addition, as observed in Fig. 9a, the IR band intensity and peak area of linear carbonyls increased during the first 20 s and then decreased slowly as a function of time, confirming that CH₄ improved the dissociation of gas phase CO₂ to produce more linear carbonyls, and the desorption of adsorbed CO (on Pt sites) was relatively slow, being consistent with previous findings.²³

As shown in the MS profile in Fig. 8a and 9a, the CO signal shows a rapid increase on the switch from CO₂ to CH₄, then the signal decreased and stabilised at a relatively lower

level compared to that measured in the presence of CO₂. Interestingly, as shown by the MS profiles in Fig. 8b and 9b, by switching back the feed to CO₂ (from CH₄), the intensity of CO signal stabilised at a higher level than that achieved under the previous condition with CO₂ after the surge. Hence, one can conclude that the formation of CO was mainly due to the consumption of the weakly surface adsorbed bidentate carbonates, which led to a decrease in the IR peak area of these species in the absence of CO₂. Specifically, for the Pt–Ni@CeO₂ catalyst (Fig. 9b), under CO₂, the intensity of the CO MS signal ($\sim 1.5 \times 10^5$) was relatively higher than that of the Ni@CeO₂ catalyst ($\sim 1.25 \times 10^5$) and bare CeO₂ support ($\sim 0.5 \times 10^5$, Fig. 8b and S14†), suggesting the contribution of CO₂ dissociation on the Pt surface to CO formation. In addition, in the system with Ni@CeO₂ (Fig. 8a), the emergence of the H₂ signal was delayed by ~ 3 s compared to that of CO and Kr, suggesting either the relatively slow dissociation of CH₄ on Ni sites with a significantly low dispersion (about 0.9%, Table S2†) or the retention of H adatoms on the Ni surface. Consequently, extensive CH_x could result in serious coke formation, which is line with the poor stability of Ni@CeO₂, as shown in Fig. 3. Conversely, for Pt–Ni@CeO₂ (Fig. 9a), Pt doping has improved the metal dispersion significantly (to about 37.6%), which enhanced the dissociation of CH₄ on the metal surface. This is confirmed by the simultaneous development of MS signals of CO, H₂ and Kr under transient conditions (Fig. 9a, right).

In the 1st cycle, for switching CH₄ back to CO₂, as shown in Fig. 8b and 9b for Ni@CeO₂ and Pt–Ni@CeO₂, respectively, the

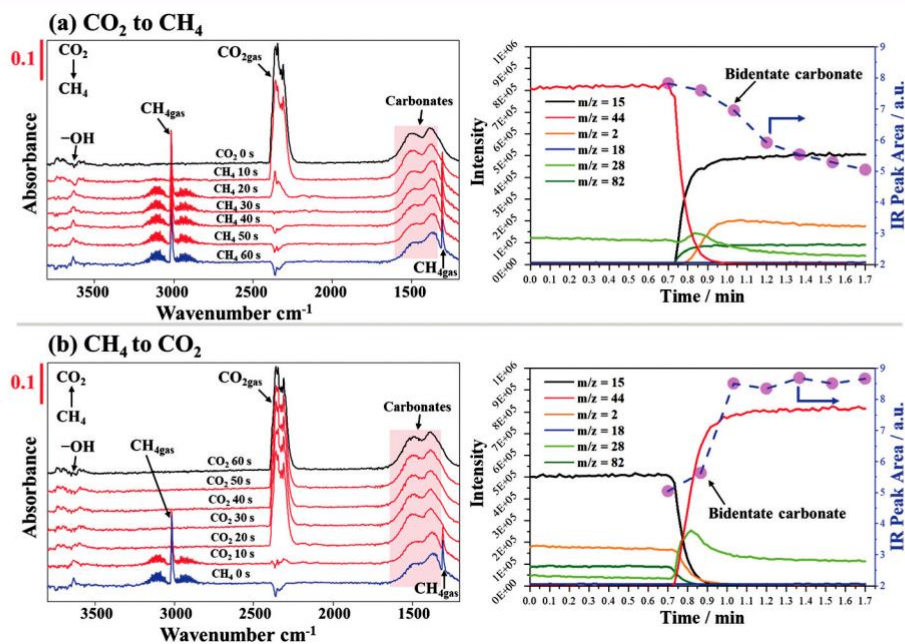


Fig. 8 In situ DRIFT spectra over the Ni@CeO₂ catalyst and corresponding MS signals collected at the exit of the DRIFTS cell and the evolution of surface bidentate carbonate and linear carbonyls as a function of ToS during the 1st cycle of the DRM process switching between CO₂ and CH₄ feeds at 550 °C: (a) CO₂ to CH₄, and (b) CH₄ to CO₂. (Experimental conditions: feed gas = 10 vol%CO₂/90 vol% Ar and feed gas = 10 vol%CH₄/30 vol% Kr/60 vol% Ar, total flow rate = 50 mL (STP) min⁻¹).

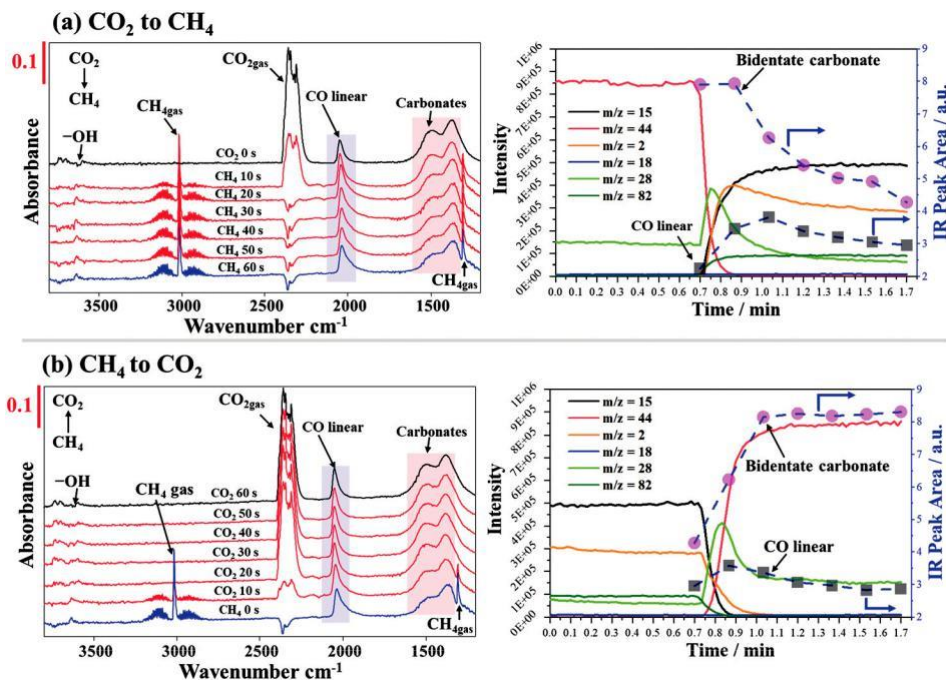


Fig. 9 In situ DRIFT spectra over the Pt–Ni@CeO₂ catalyst and corresponding MS signals collected at the exit of the DRIFTS cell and the evolution of surface bidentate carbonate and CO carbonyls as a function of ToS during the 1st cycle of the DRM process switching between CO₂ and CH₄ feeds at 550 °C: (a) CO₂ to CH₄, and (b) CH₄ to CO₂. (Experimental conditions: feed gas = 10 vol%CO₂/90 vol% Ar and feed gas = 10 vol%CH₄/30 vol% Kr/60 vol% Ar, total flow rate = 50 mL (STP) min⁻¹).

progression of the surface species and peak area of surface bidentate carbonate showed transposed phenomena. However, for the CO MS signal, a similar fluctuation, that is, an immediate surge after the feed switch, was measured for the Pt–Ni@CeO₂ catalyst (Fig. 9), which corresponds well to the evolution of the IR band intensity and peak area of linear carbonyls on the catalyst surface. Repeatable results were obtained under the conditions used, as shown in Fig. S15–S18.†

To gain more information on the linear carbonyls adsorbed on the surface of the Pt–Ni@CeO₂ catalyst, DRIFT spectra in the region of 1880–2100 cm⁻¹ (recorded during the 1st cycle under fast cycling transient conditions) were studied in detail as shown in Fig. 10. Fig. 10a shows that the characteristic band at about 2040 cm⁻¹, which is associated with linear Pt⁰–CO species, slightly fluctuated upon switching the feed between CO₂ and CO₂/CH₄. Conversely, for the system of switching between CO₂ and CH₄ (Fig. 10b), the surface CH_x species (from CH₄ dissociation) adsorbed on the bimetallic Pt–Ni sites could shift the band location of surface carbonyls towards lower frequencies.

Reaction mechanisms and pathways. Based on the fast cycling transient in situ DRIFTS-MS studies above, the plausible reaction pathways were proposed for catalytic DRM over the monometallic Ni@CeO₂ and bimetallic Pt–Ni@CeO₂ catalysts, which are presented in Fig. 11. For both catalysts, identical reaction pathways were proposed, i.e., (i) CH₄ first adsorbed on the Ni sites and then dissociated further to generate a CH_x species, which then rapidly decomposed to give C and H adatoms. Subsequently, H adatoms could

diffuse and react with lattice oxygen of CeO₂ to produce –OH groups, which may further combine with H adatoms to produce H₂O and H₂. Meanwhile, the –OH groups could also spillover H onto the surface of the metal to form H₂. Finally, the surface C can either react with lattice oxygen close to the metal–CeO₂ interface to form CO or coke on the metal surface;²³ (ii) CO₂ can either react with lattice oxygen on CeO₂ to form bidentate and polydentate carbonates, generating more lattice oxygen for replenishing oxygen in CeO₂ which was removed by the reaction with C dissociated from CH₄ according to a previous study.²³ Specifically, according to the transient DRIFTS-MS results (Fig. 8 and 9), surface bidentate carbonates could be the possible reactive surface intermediates, which can rapidly decompose to form CO and to replenish lattice oxygen for the CeO₂ support.²³ However, surface polydentate carbonates are relatively stable and hard to dissociate,^{37,40} which could be the spectators during the catalysis, being consistent with previous findings.⁷ In addition to the reaction pathways proposed for Ni and CeO₂ surfaces, over the bimetallic Pt–Ni@CeO₂ catalyst (Fig. 11b), CO₂ can also dissociate on the surface of Pt sites to form weakly adsorbed linear carbonyls, and subsequently desorbed to produce CO. Importantly, the surface O adatoms dissociated from CO₂ can simultaneously remove surface C from the CH₄ dissociation to prevent coking during the reaction, interpreting the significantly improved anti-coking performance of the bimetallic Pt–Ni catalyst compared to the monometallic Ni catalyst, which has been proved by the longevity test (Fig. 3, and previous findings²²).

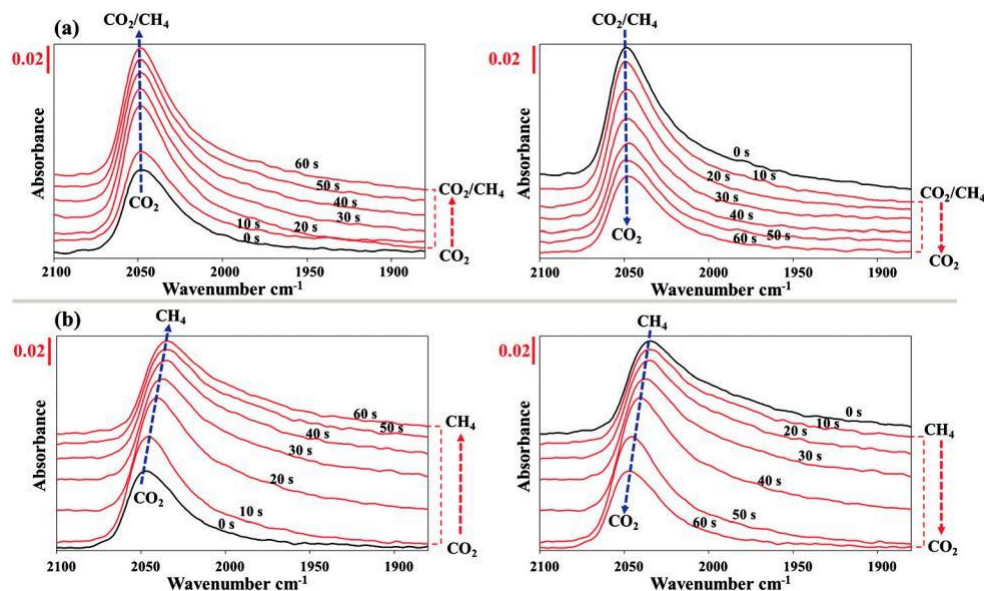


Fig. 10 Detailed DRIFT spectra of surface carbonyls over the Pt-Ni@CeO₂ catalyst as a function of ToS in the transient DRM experiments at 550 °C with (a) feed switching between CO₂ and CO₂/CH₄, and (b) feed switching between CO₂ and CH₄. (Experimental conditions: feed gas = 10 vol%CO₂/90 vol% Ar and feed gas = 10 vol%CH₄/30 vol% Kr/60 vol% Ar, feed gas = 10 vol%CO₂/10 vol%CH₄/30 vol% Kr/50 vol% Ar (when added), total flow rate = 50 mL (STP) min⁻¹).

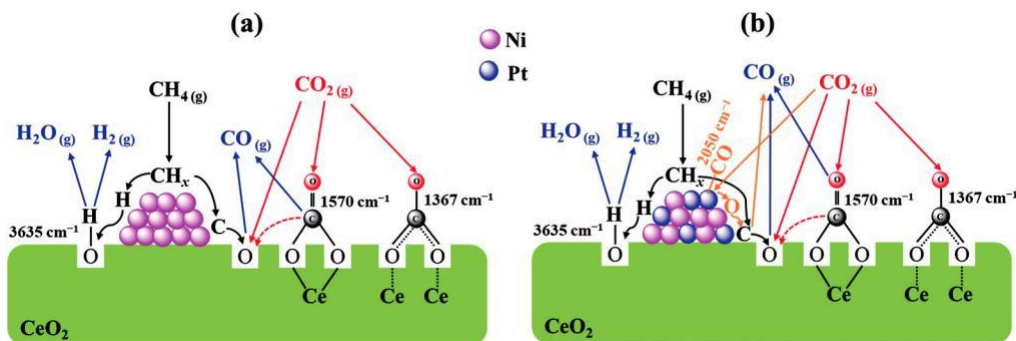


Fig. 11 Schematic representation of the plausible reaction mechanism for catalytic DRM over different catalysts under investigation: (a) Ni@CeO₂ and (b) Pt-Ni@CeO₂.

4. Conclusions

Dry reforming of methane (DRM) has attracted great attention in the catalysis community due to its two-fold potential for converting greenhouse gases of CO₂ and CH₄ to value-added syngas. Bimetallic Pt-Ni catalysts are highly active and coke resistant for promoting catalytic DRM in comparison with monometallic Ni catalysts. Here, DRM over Ni and Pt-Ni supported on ceria catalysts (i.e., Ni@CeO₂ and Pt-Ni@CeO₂) was studied in situ by DRIFTS-MS characterisation to understand the improved activity and anti-deactivation ability of the bimetallic Pt-Ni@CeO₂ catalyst (in comparison with the monometallic Ni@CeO₂ catalyst). Under temperature-ramping (from 50 to 600 °C) and isothermal steady-state (at 550 °C) conditions, various surface species were detected on the catalysts under

investigation. Subsequently, fast cycling transient experiments (switching between CO₂ and CO₂/CH₄, and CO₂ and CH₄, with a short duration of 1 min for each cycle, at 550 °C) revealed that -OH groups, linear carbonyls and bidentate carbonates were the active surface intermediates during DRM, whilst polydentate carbonates were the inactive spectators.

Accordingly, identical DRM reaction pathways were proposed for both Ni@CeO₂ and Pt-Ni@CeO₂ catalysts, i.e. (i) CH₄ mainly dissociated on the surface of metal sites to produce surface adatoms C and H, which subsequently diffused on the surface of the catalysts and reacted with lattice oxygen donated by CeO₂ to generate CO and -OH groups (specifically, the -OH groups can possibly combine with H to form H₂O). The existence of Pt sites in the

bimetallic catalyst could significantly improve metal dispersion, and thus facilitate the decomposition of CH₄; and (ii) CO₂ mainly combined with lattice oxygen to form bidentate carbonates, and subsequently dissociated to form CO. Significantly, the existence of Pt sites in the bimetallic catalyst could facilitate the decomposition of CO₂ to produce CO- and oxygen-adsorbed species, and subsequently the surface oxygen could purge the surface carbon derived from CH₄ decomposition, endowing the bimetallic Pt–Ni catalyst with significantly improved anti-coking properties. Meanwhile, the decomposition of CO₂ on Pt sites also facilitated the formation of CO, giving the plausible reason for the relatively low H₂/CO molar ratio (~0.65) achieved by the Pt–Ni catalyst.

Conflicts of interest

There are no conflicts to declare.

Acknowledgements

HC is thankful for the financial support from the Jiangsu Specially-Appointed Professors Program, the Natural Science Foundation of Jiangsu Province (BK20200704). SX is thankful for the financial support from the Dean's Doctoral Scholar Awards from the University of Manchester. UK Catalysis Hub is kindly acknowledged for resources and support provided via our membership of the UK Catalysis Hub Consortium and funded by EPSRC grant: EP/R026939/1, EP/R026815/1, EP/R026645/1, and EP/R027129/1.

References

- 1 M. Yu, K. Zhu, Z. Liu, H. Xiao, W. Deng and X. Zhou, *Appl. Catal., A*, 2014, 148–149, 177–190.
- 2 A. Sternberg, C. M. Jens and A. Bardow, *Green Chem.*, 2017, 19, 2244–2259.
- 3 J. L. Ewbank, L. Kovarik, C. C. Kevlin and C. Sievers, *Green Chem.*, 2014, 16, 885–896.
- 4 W.-J. Jang, J.-O. Shim, H.-M. Kim, S.-Y. Yoo and H.-S. Roh, *Catal. Today*, 2019, 324, 15–26.
- 5 J. R. Rostrup-Nielsen, *Catal. Today*, 1997, 37, 225–232.
- 6 M. Bradford and M. Vannice, *Catal. Rev.: Sci. Eng.*, 1999, 41, 1–42.
- 7 Z. Liu, F. Zhang, N. Rui, X. Li, L. Lin, L. E. Betancourt, D. Su, W. Xu, J. Cen, K. Attenkofer, H. Idriss, J. A. Rodriguez and S. D. Senanayake, *ACS Catal.*, 2019, 9, 3349–3359.
- 8 S. M. Kim, P. M. Abdala, T. Margossian, D. Hosseini, L. Foppa, A. Armutlulu, W. van Beek, A. Comas-Vives, C. Copéret and C. Müller, *J. Am. Chem. Soc.*, 2017, 139, 1937–1949.
- 9 J. Dou, R. Zhang, X. Hao, Z. Bao, T. Wu, B. Wang and F. Yu, *Appl. Catal., A*, 2019, 254, 612–623.
- 10 S. Zhang, S. Muratsugu, N. Ishiguro and M. Tada, *ACS Catal.*, 2013, 3, 1855–1864.
- 11 J. R. Rostrupnielsen and J. H. B. Hansen, *J. Catal.*, 1993, 144, 38–49.
- 12 A. Á. M, L. F. Bobadilla, V. Garcilaso, M. A. Centeno and J. A. Odriozola, *J. CO₂ Util.*, 2018, 24, 509–515.
- 13 T. D. Gould, M. M. Montemore, A. M. Lubers, L. D. Ellis, A. W. Weimer, J. L. Falconer and J. W. Medlin, *Appl. Catal., A*, 2015, 492, 107–116.
- 14 Y. Mukainakano, K. Yoshida, S. Kado, K. Okumura, K. Kunimori and K. Tomishige, *Chem. Eng. Sci.*, 2008, 63, 4891–4901.
- 15 S. R. de Miguel, I. M. J. Vilella, S. P. Maina, D. San José-Alonso, M. C. Román-Martínez and M. J. Illán-Gómez, *Appl. Catal., A*, 2012, 435–436, 10–18.
- 16 D. Liu, W. N. E. Cheo, Y. W. Y. Lim, A. Borgna, R. Lau and Y. Yang, *Catal. Today*, 2010, 154, 229–236.
- 17 Z. Xie, B. Yan, J. H. Lee, Q. Wu, X. Li, B. Zhao, D. Su, L. Zhang and J. G. Chen, *Appl. Catal., A*, 2019, 245, 376–388.
- 18 W.-J. Cai, L.-P. Qian, B. Yue and H.-Y. He, *Chin. Chem. Lett.*, 2014, 25, 1411–1415.
- 19 M. Ocsachoque, F. Pompeo and G. Gonzalez, *Catal. Today*, 2011, 172, 226–231.
- 20 C. Crisafulli, S. Scirè, S. Minicò and L. Solarino, *Appl. Catal., A*, 2002, 225, 1–9.
- 21 J. H. Jeong, J. W. Lee, D. J. Seo, Y. Seo, W. L. Yoon, D. K. Lee and D. H. Kim, *Appl. Catal., A*, 2006, 302, 151–156.
- 22 D. G. Araiza, D. G. Arcos, A. Gómez-Cortés and G. Díaz, *Catal. Today*, 2021, 360, 46–54.
- 23 A. M. O'Connor, F. C. Meunier and J. R. H. Ross, in *Studies in Surface Science and Catalysis*, ed. A. Parmaliana, D. Sanfilippo, F. Frusteri, A. Vaccari and F. Arena, Elsevier, 1998, vol. 119, pp. 819–824.
- 24 L. F. Bobadilla, V. Garcilaso, M. A. Centeno and J. A. Odriozola, *ChemSusChem*, 2017, 10, 1193–1201.
- 25 B. Wichterlová, P. Sazama, J. P. Breen, R. Burch, C. J. Hill, L. Čapek and Z. Sobalík, *J. Catal.*, 2005, 235, 195–200.
- 26 S. Chansai, R. Burch, C. Hardacre, J. Breen and F. Meunier, *J. Catal.*, 2011, 281, 98–105.
- 27 S. Chansai, R. Burch, C. Hardacre, H. Oh and W. S. Epling, *Catal. Sci. Technol.*, 2013, 3, 2349–2356.
- 28 S. Chansai, R. Burch, C. Hardacre, J. Breen and F. Meunier, *J. Catal.*, 2010, 276, 49–55.
- 29 X. Wang, H. Shi, J. H. Kwak and J. Szanyi, *ACS Catal.*, 2015, 5, 6337–6349.
- 30 B. Miao, S. S. K. Ma, X. Wang, H. Su and S. H. Chan, *Catal. Sci. Technol.*, 2016, 6, 4048–4058.
- 31 F. Romero-Sarria, L. F. Bobadilla, E. M. J. Barrera and J. A. Odriozola, *Appl. Catal., B*, 2020, 119032, DOI: 10.1016/j.apcatb.2020.119032.
- 32 S. Chansai, R. Burch and C. Hardacre, *J. Catal.*, 2012, 295, 223–231.
- 33 S. Chansai, R. Burch, C. Hardacre, D. Norton, X. Bao and L. Lewis, *Appl. Catal., B*, 2014, 160–161, 356–364.
- 34 S. Chansai, R. Burch, C. Hardacre and S. Naito, *J. Catal.*, 2014, 317, 91–98.
- 35 H. Chen, Y. Shao, Y. Mu, H. Xiang, R. Zhang, Y. Chang, C. Hardacre, C. Wattanakit, Y. Jiao and X. Fan, *AIChE J.*, 2021, 67, e17126.

- 36 Z. Xie, B. Yan, S. Kattel, J. H. Lee, S. Yao, Q. Wu, N. Rui, E. Gomez, Z. Liu, W. Xu, L. Zhang and J. G. Chen, *Appl. Catal., B*, 2018, 236, 280–293.
- 37 L. Lin, S. Yao, Z. Liu, F. Zhang, N. Li, D. Vovchok, A. Martínez-Arias, R. Castañeda, J. Lin, S. D. Senanayake, D. Su, D. Ma and J. A. Rodriguez, *J. Phys. Chem. C*, 2018, 122, 12934–12943.
- 38 O. Pozdnyakova, D. Teschner, A. Wootsch, J. Kröhnert, B. Steinhauer, H. Sauer, L. Toth, F. C. Jentoft, A. Knop-Gericke, Z. Paál and R. Schlögl, *J. Catal.*, 2006, 237, 17–28.
- 39 S. Kattel, B. Yan, J. G. Chen and P. Liu, *J. Catal.*, 2016, 343, 115–126.
- 40 K. Yoshikawa, H. Sato, M. Kaneeda and J. N. Kondo, *J. CO₂ Util.*, 2014, 8, 34–38.